Formation of blade and slot die coated small molecule multilayers for OLED applications studied theoretically and by XPS depth profiling

Katharina Peters, Sebastian Raupp, Helga Hummel, Michael Bruns, Philip Scharfer, and Wilhelm Schabel

Citation: AIP Advances **6**, 065108 (2016); doi: 10.1063/1.4953845
View online: http://dx.doi.org/10.1063/1.4953845
View Table of Contents: http://scitation.aip.org/content/aip/journal/adva/6/6?ver=pdfcov
Published by the AIP Publishing

Formation of blade and slot die coated small molecule multilayers for OLED applications studied theoretically and by XPS depth profiling

Katharina Peters,[1] Sebastian Raupp,[1,a] Helga Hummel,[2] Michael Bruns,[3] Philip Scharfer,[1] and Wilhelm Schabel[1]
[1]*Institute of Thermal Process Engineering, Thin Film Technology, Karlsruhe Institute of Technology (KIT), Karlsruhe, Germany*
[2]*Philips Technologie GmbH Innovative Technologies, Aachen, Germany*
[3]*Institute for Applied Materials and Karlsruhe Nano Micro Facility (KNMF), Karlsruhe Institute of Technology (KIT), Karlsruhe, Germany*

(Received 22 January 2016; accepted 30 May 2016; published online 8 June 2016)

Slot die coaters especially designed for low material consumption and doctor blades were used to process small molecule solutions for organic light-emitting diodes (OLEDs). Optimum process parameters were developed for the large-scale coating techniques to generate stable single and multiple layers only a few nanometers thick. Achieving a multilayer architecture for solution-processed OLEDs is the most challenging step. X-ray photoelectron spectroscopy sputter depth profiling was performed to determine defined interfaces between coated organic layers. Commercially available small molecules NPB (N,N'-Di(1-naphthyl)-N,N'-diphenyl-(1,1'-biphenyl)-4,4'-diamine) and BAlq (Bis(8-hdroxy-2methylquinoline)-(4-phenylphenoxy)aluminum), originally developed for vacuum deposition, were used as hole, respectively electron transport material. Defined double-layers were processed with both scalable coating methods using the orthogonal solvent approach. The use of non-orthogonal solvents resulted in complete intermixing of the material. The results are explained by calculations of solubilities and simulating drying and diffusion kinetics of the small molecule solutions.
[http://dx.doi.org/10.1063/1.4953845]

I. INTRODUCTION

Organic light-emitting diodes (OLEDs) consist of several functional layers with layer thicknesses in the range of 5 to 100 nm. Small molecule active material is used for the most efficient devices.[1,2] Evaporation techniques[3] and solution processing[4] can be applied for the manufacturing of multilayer OLED devices. Solution processing offers the possibility of reducing the production time and costs[5–7] and is a standardized process in several industrial applications. The material yield is significantly higher compared to evaporated functional layers. Lab scale spin coating is the state-of-the-art coating technology for solution-processed OLED layers. Doctor bladed devices are compared with spin-coated or evaporated ones elsewhere.[8,9] The challenge in solution processing is to prohibit the intermixing of the functional layers. Sharp and defined interfaces are required for the high efficiency of the device.[10] Undefined interfaces lead to a loss of the function separation[11] and a shift of the area for electron-hole recombination. The low film thicknesses in organic electronics applications and the high requirements for the quality of the interfaces demand extremely precise coating techniques.[12]

[a]sebastian.raupp@kit.edu, +49 721 608 43950

Coating one layer on top of another can lead to an etching of the bottom layer caused by the solvent of the top layer.[7] Several approaches in literature describe a possible prevention of the dissolution and intermixing especially for OLED systems.[13] One of the most promising approaches is the orthogonal solvent one[14] investigated for laboratory method spin coating.[4,15–17] According to this approach, the second layer is applied while using a solvent in which the material of the first layer is insoluble. The confinements are that the solubilities of the semiconductor materials cannot be varied in a wide range without changing the electric properties and that most solvents show a low solubility. However, a low solubility was found to be sufficient to lead to an intermixing of OLED material.[18] Nevertheless, devices with a spin-coated emissive host system onto a hole transport layer using a non-orthogonal solvent were also presented in literature, where only a reduced layer thickness[19,20] or a small shift in the electroluminescent spectra, caused by a possible small mixing zone, were described.[21] A solvent is considered to be non-orthogonal if it is possible to dissolve both solids applied to a larger extent in the solvent itself. In addition to the solubility aspects, the coating and drying conditions are also of importance. With a fast drying process, the diffusion time can be reduced and intermixing of the material might be prevented. This was described as a possible tool to suppress the intermixing of spin or blade-spin coated layers.[22,23]

In this work, we aim at investigating precise large area coating techniques for small molecule OLED multilayers under defined drying conditions. Subsequent doctor blading and slot die coating was applied using N,N'-Di(1-naphthyl)-N,N'-diphenyl-(1,1'-biphenyl)-4,4'-diamine (NPB) and Bis(8-hdroxy-2methylquinoline)-(4-phenylphenoxy)aluminum (BAlq) as solutes and different solvents with low and non-orthogonal solubility. The NPB is mainly used as a host molecule for the emissive layer or hole transport layer.[24–26] The BAlq is typically used as an electron transport layer or hole-blocking layer, respectively.[27,28] X-ray photoelectron spectroscopy (XPS) sputter depth profiling was performed in order to prove the layer uniformity with sharp interfaces, and the homogeneous elemental distribution of such solution-processed organic multilayers in comparison to well-known evaporated systems. The characterization technique is used in literature to investigate evaporated organic or anorganic[29] and spin-coated organic layers.[30] Other common techniques for the analysis of thin organic layers which do not provide the information about the local layer composition, such as atomic force microscopy, white light interferometry and measurement of layer thickness, are not applicable.

II. EXPERIMENTAL & METHODS

A. Materials

The commercially available materials NPB (Figure 1(a)) (CAS 123847-85-8, purity 96 %, SigmaAldrich, Schnelldorf, Germany) and BAlq (Figure 1(b)) (CAS 146162-54-1, purity 95 %, VWR, Darmstadt, Germany) were selected as solutes. Toluene (TOL; HPLC grade, VWR, Darmstadt, Germany) was used for the deposition of NPB ($c_{NPB,TOL}$ = 5 mg/ml) and BAlq was coated with ethanol (EtOH; HPLC grade, VWR, Darmstadt, Germany) ($c_{BAlq,EtOH}$ = 5 mg/ml) or TOL ($c_{BAlq,TOL}$ = 5 mg/ml).

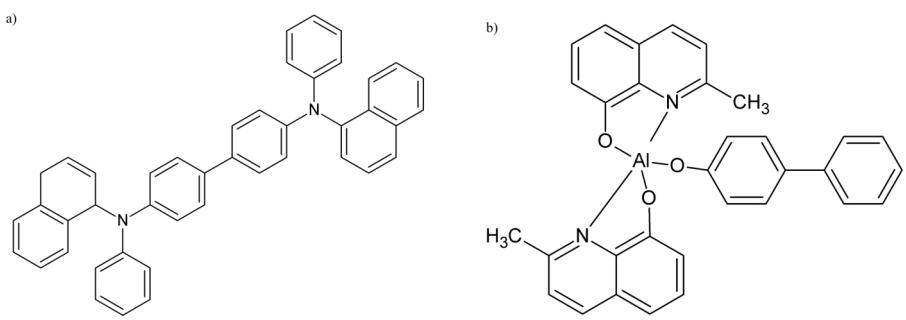

FIG. 1. Chemical structure of the organic material used: 1(a) NPB, 1(b) BAlq.

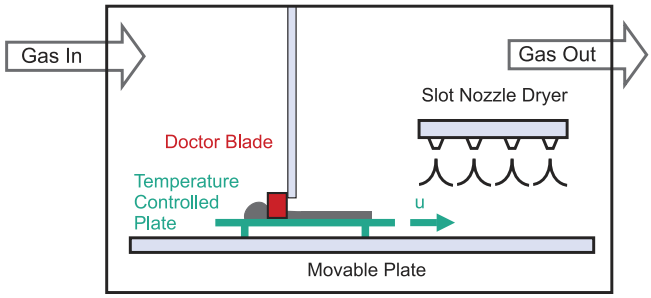

FIG. 2. Batch coater with temperature-controlled coating table and fixed doctor blade.[32]

B. Coating and drying of solution-processed samples

Experiments were performed in a self-constructed batch coater (Figure 2). Layers were coated using a doctor blade (ZUA 2000, Zehntner AG, Switzerland) with an accessible coating width of 60 mm or a slot die coater with a determined coating width of 35 mm onto float glass (LxWxH: 60 x 30 x 1 mm^3 or 300 x 60 x 1 mm^3). The glass with the sample was cut into 10 x 10 mm^2 sized pieces for XPS measurements. The temperature of the coating table was adjusted to 60 °C via a cryostatic temperature regulator (LAUDA RP855C) with water as the heating/cooling medium.

The properties of the highly dilute solutions of small molecules correspond almost exactly to those of the pure solvents, placing high demands on the coating processes. Parameters were chosen within the stable process window for the self-metered blade coating and pre-metered slot die coating.[31] Optimal parameters for the velocity and the volume of second layer solution provided have to be used for blade coating to reduce the amount of removal of the dry first layer. A gap between glass and blade of 70 µm was selected and a volume of 40 µL (first layer) or 20 µl (second layer) was deposited in front of the fixed blade as standard parameters, while the coating table was subsequently moved with a velocity of 100 mm/s. The volume flow required for slot die coating can be set initially, thus, the liquid feed reservoir and contact of solvent of the second layer with the dry material is reduced concurrently. The slot die was mounted on a sliding carriage so that the substrate could be moved underneath. A gap of 191 µm was adjusted between the substrate and the fixed slot die. A volume flow rate of 0.5 ml/min regulated by a syringe pump and a coating table velocity of 15 mm/s were chosen as parameters. With these parameters, a wet layer film with a thickness of 15 µm as the first layer or 10 µm as the second layer for doctor blading was produced.

The samples were dried by moving the plate under a slot nozzle dryer providing a heat transfer coefficient of 10 $W/(m^2 \cdot K)$. The movable plate was oscillated continuously to avoid local differences in the drying conditions.

Samples were fabricated according to two different methods. NPB was blade coated as the first layer from TOL and dried. Two different BAlq solutions were deposited by blade, respectively slot die coating, onto two prepared NPB layers. In method 1, the BAlq layer was applied from EtOH solution, following the orthogonal approach with a low solubility for NPB of 0.1 mg/ml or 0.013 wt.-%, and in method 2, from TOL solution (solubility for NPB approximately 10 mg/ml or 1.16 wt.-%).

C. X-ray photoelectron spectroscopy

X-ray photoelectron spectroscopy measurements were performed using a K-Alpha XPS spectrometer (ThermoFisher Scientific, East Grinstead, UK). Data acquisition and processing using the Thermo Avantage software is described elsewhere.[33] All samples were analyzed using a micro-focused, monochromated Al Kα X-ray source (30 – 400 µm spot size). The K-Alpha charge compensation system was employed during analysis, using electrons of 8 eV energy and low-energy argon ions to prevent any localized charge build-up. The spectra were fitted with one or more Voigt profiles (binding energy uncertainty: +/- 0.2eV). The analyzer transmission function, Scofield sensitivity factors[34] and effective attenuation lengths (EALs) for photoelectrons were applied for

quantification. The EALs were calculated using the standard TPP-2M formalism.[35] All spectra were referenced to the C1s peak of hydrocarbon at 285.0 eV binding energy controlled by means of the well-known photoelectron peaks of metallic Cu, Ag and Au.

Sputter depth profiles were performed using a raster scanned Argon-Ion beam at 3.0 keV and 30° angle of incidence. The atomic concentration is plotted versus the sputter time, because the sputter depth for mixtures with unknown composition cannot be obtained.

D. Evaporated reference samples

Two different reference samples with a thickness of 120 nm were produced via vacuum deposition. For a sample with defined interfaces, 60 nm of BAlq was evaporated subsequently onto the NPB layer (Figure 3(a)). A completely mixed layer was processed by evaporating a 1:1 mixture of NPB and BAlq as a second reference (Figure 3(b)). The atomic compositions are important for the differentiation of the material with XPS measurements. The BAlq ($C_{32}H_{25}AlN_2O_3$) contains carbon, nitrogen and hydrogen similar to NPB ($C_{44}H_{32}N_2$), but also aluminum and oxygen. The substrate (float glass: Si, O) can be distinguished from the organic layers by silicon and a high amount of oxygen. In our experiments, therefore, we analyzed especially the oxygen and aluminum concentration over sputter time as an indicator of the sharp interfaces or intermixing, respectively.

It is well-known that XPS sputter depth profiling of organic materials using mono Ar^+ ion beams induces degradation and loss of the chemical information, which can only be overcome by Ar cluster ion sputtering.[36] Nevertheless, Figure 4(a) doubtlessly evidences this procedure as a suitable means to characterize multilayer stacks of different organic layers with respect to the elemental distribution and the sharpness of interfaces and to prove intermixing of adjacent layers, cf. Figure 4(b). In particular, the Al and O content of BAlq (C-84, O-8, N-5, Al-3) and even the variation of the N content within BAlq and NBP (C-96, N-4), respectively, can clearly act as markers for the different layers. Due to the high concentration of carbon within the OLED layers and of Si in the glass substrate, these components are not shown for a better visualization. In conclusion, XPS sputter depth profiling is a powerful tool to characterize solution-processed layer stacks.

The XPS sputter profiles need to be compared with the reference sputter profiles to judge whether a sharp interface has been created. Due to the evaporation process, the double-layer reference device has no intermixing zone. The atomic concentration of Al, O and N is analyzed to judge whether a sharp interface has been created or not. As shown in Figure 4(a), the changes in atomic concentrations of all marker atoms take place at a sputter time of ~260 s in a time interval of approximately 20 s. It is not an immediate change in the concentration profiles due to the resolution of the XPS technique of several nanometers. The Al concentration, for example, drops rapidly from almost 3.5 to 0 %. The sputtering process for the mixture illustrated in Figure 4(b) shows the same total sputter time compared to the double layer in Figure 4(a). The sharp decrease of C atomic concentration for both samples takes place after ~700 s. Oxygen concentration increases rapidly and, therefore, the underlying glass substrate is detected.

E. Modeling of solubility, diffusion and drying

Calculations for both solvents were performed to investigate the influence of solubility, determined by the phase equilibrium. A 60 nm thick NPB film together with a solvent wet film of

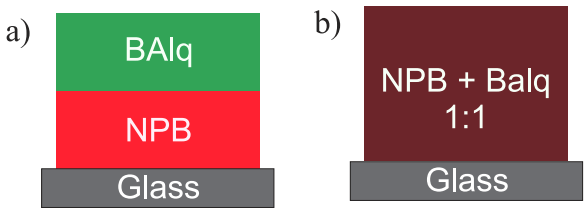

FIG. 3. Architecture of references (schematic): 3(a) double layer, 3(b) mixed layer.

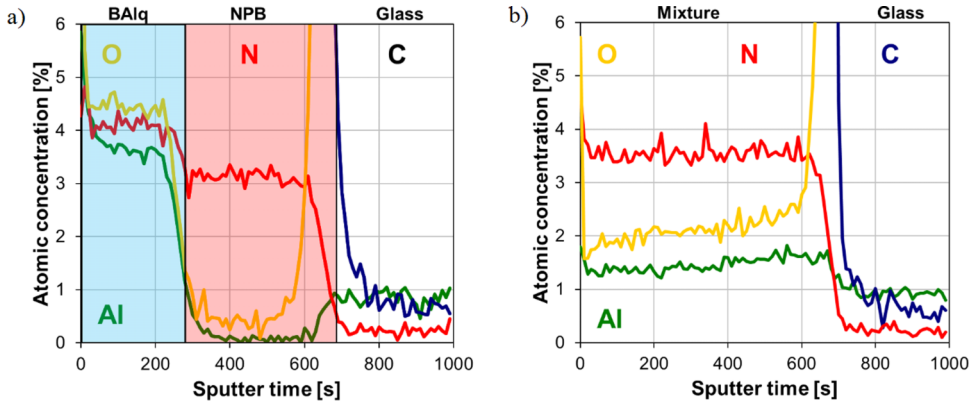

FIG. 4. XPS sputter depth profiles of BAlq and NPB reference layers evaporated onto glass substrates: 4(a) multilayer consisting of pure BAlq and NBP indicating a defined interface, 4(b) single layer consisting of a 1:1 mixture of NPB and BAlq.

h_{wet} = 10 µm were analyzed for the calculations. With the measured saturation of 0.1 mg/ml NPB in EtOH and 10 mg/ml in TOL, the film thickness of NPB which can be dissolved was calculated. As shown in Figure 5, only a small amount of NPB can be dissolved in EtOH (~ 0.8 nm; Figure 5, left) while the 60 nm are completely dissolved in TOL (Figure 5, right).

The NPB-EtOH solution is saturated. By contrast, the 10 µm thick TOL film is still able to dissolve more NPB before reaching the phase equilibrium and is not saturated. More information about the calculations can be found in the supplemental material A.[37]

A simulation was implemented in visual basic to estimate diffusion and drying kinetics. The calculation of diffusional intermixing was based on a one-dimensional simulation with the finite differences method. In the model, a solvent film with the height h_{wet} = 10 µm is placed on a solid film with the height h_{solid} = 60 nm. The solid diffuses in the solvent film due to the concentration gradient in the film. The first film element at the interface between solid and solvent is assumed to be in phase equilibrium. Thus, the solid concentration equals its saturation. This is shown in Figure 6.

As a worst case approximation, film shrinkage due to drying is neglected. This results in an overestimation of the dissolution kinetics of the solid film due to more solvent being present in the calculation than in reality. If changing the drying kinetics could influence the intermixing can be estimated by comparing the time it takes for the system to diffuse and the drying time. A volumetric coordinate system was chosen. A mass balance for an infinite volume element i was set up (eq. (1)) describing the diffusion with Fick's law:

$$\frac{\partial c_i}{\partial t} = -\frac{\partial}{\partial z}\left(-D \cdot \frac{\partial c_i}{\partial z}\right) = D \cdot \frac{\partial^2 c_i}{\partial z^2} \tag{1}$$

The discretization is approximated via:

$$\frac{c_{z,t+1} - c_{z,t}}{\Delta t} = D \cdot \frac{c_{z+1,t} + c_{z-1,t} - 2c_{z,t}}{\Delta z^2} \tag{2}$$

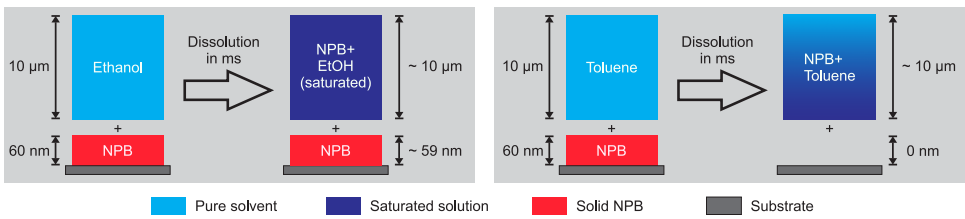

FIG. 5. Dissolution of 60 nm NPB film in ethanol (EtOH; left) and in toluene (TOL; right).

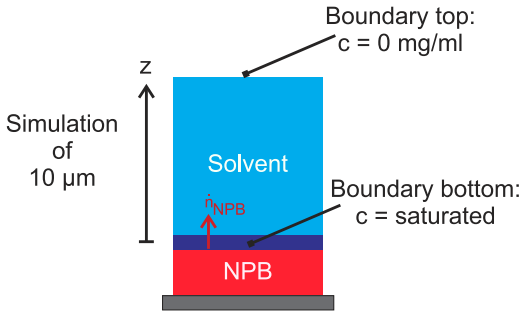

FIG. 6. Model for the simulation of the diffusion of a 60 nm NPB film into a 10 µm thick wet solvent film. The NPB is diffusing into the solvent due to a saturated film element on the bottom of the wet film (boundary condition).

The module M (eq. (3)) is introduced as a stability criterion (Ref. 38). The method is regarded as stable for values of M < 0.5 (38).

$$M = \frac{D \cdot \Delta t}{\Delta z^2} \leq \frac{1}{2} \tag{3}$$

We use M = 0.1 for our calculations to ensure a stable routine.

Based on the known concentrations of the component of interest for the elements z, z+1 and z-1 for the concentration at the point of time t, the concentration at height z for the point of time t+1 can be calculated (eq. (3) inserted in eq. (2).):

$$c_{z,t+1} = M \cdot c_{z-1,t} + M \cdot c_{z+1,t} + (1 - 2M) \cdot c_{z,t} \tag{4}$$

The concentration can be plotted for every film element as a function of time. If the drying time is higher than the time for the diffusion and, respectively, dissolution, intermixing occurs.

The drying rate was calculated for the experimental conditions and an approximated heat transfer coefficient of 10 W/(m^2·K). The calculations are based on the Stefan-Maxwell diffusion equations solved for the binary system with one-sided diffusion[39] (eq. (5)). The flux of evaporated solvent is given as follows:

$$\dot{n}_i = \beta_{ig} \cdot \tilde{\rho}_g \cdot \tilde{y}_{i,Ph} = \frac{\alpha}{\tilde{c}_{p,i} \cdot Le^{1-n}} \cdot (\tilde{y}_{i,Ph} - \tilde{y}_{i,\infty}) \tag{5}$$

No accumulation of solvent takes place in the air due to the air flux in the dryers, which results in $\tilde{y}_{i,\infty} = 0$.

The phase equilibrium of the organic solvent in the solution is determined with the UNIFAC model.[38] The behavior of the solution can be described approximately as pure solvent. The drying rate $\dot{m}_i$ is calculated via eq. (6). The drying rate can be calculated from the wet-film thickness known from the process parameters for slot die coating and the density of the solvent (eq. (7)).

$$\dot{m}_i = \dot{n}_i \cdot \tilde{M}_i \tag{6}$$

$$t_{dry} = \frac{h_{wet}}{\dot{m}_i / \rho_i} \tag{7}$$

The linear dependence of drying time from the heat transfer coefficient α and the wet film thickness h_{wet} arises from eq. (5) and (7). More information about the parameters for the simulation can be found in the supplemental material section B.[37]

III. RESULTS

Solution-processed samples were prepared with two scalable coating methods as described in the experimental section. Homogeneous multilayers can be obtained with both coating tools. The experimental results are validated by calculations of drying and diffusion kinetics.

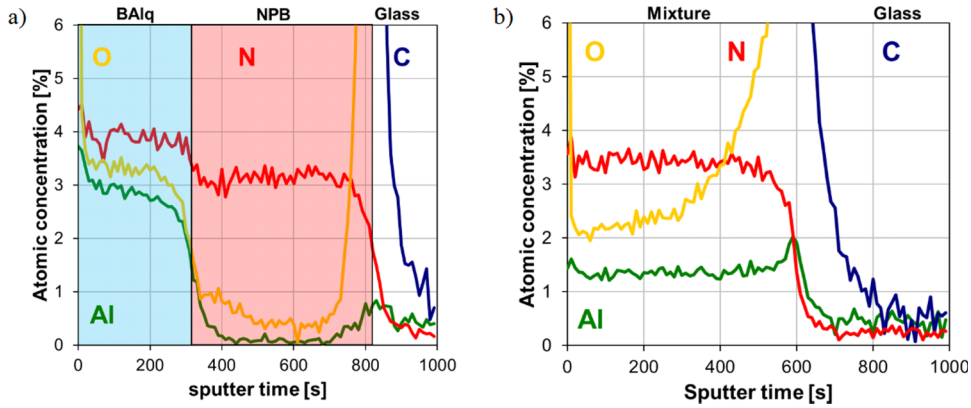

FIG. 7. XPS sputter depth profiles of doctor bladed double layers of NPB and BAlq onto glass substrates: 7(a) Defined interface – BAlq is coated by EtOH as an orthogonal solvent for NPB, 7(b) Mixture – BAlq is coated by TOL as a non-orthogonal solvent for NPB.

The XPS sputter depth profiles of a doctor bladed double layer of NPB and BAlq using the orthogonal approach is presented in Figure 7(a) and clearly evidences the sharp interface achieved between the BAlq and NBP layers similar to the layer stack deposited by evaporation, cf. Figure 4(a). The sputter times until the decrease in atomic concentrations of Al, N and O appear and are almost the same as for the reference device, meaning that the interface appears at the same position. The ~60 nm thick BAlq film is sputtered first before the NPB film is measured. The decrease of atomic Al, as well as atomic N and O concentration takes place in the same time interval as for the reference device. Therefore, it can be concluded that the interface in Figure 7(a) is as sharp as for the reference device in Figure 4(a). By contrast, the usage of non-orthogonal solvents leads to completely intermixed multilayers with homogenous in-depth distribution of the marker elements, cf. Figure 7(b), corroborated by the sputter depth profile of the mixed reference sample in Figure 4(b).

Slot die coating, with better process conditions by reduced feed reservoir in front of the coating tool compared to doctor blading, leads to the same results. Separated layers can be created with this pre-metered coating method by using an orthogonal solvent, cf. Figure 8(a), while the coating conditions cannot prevent a complete intermixing in the case of non-orthogonal solvents, cf. Figure 8(b). Again, the sharpness of interfaces in Figure 8(a) can be estimated to be the same as for the reference device. The interface is found to appear at a sputter time of ~220 s, which is slightly

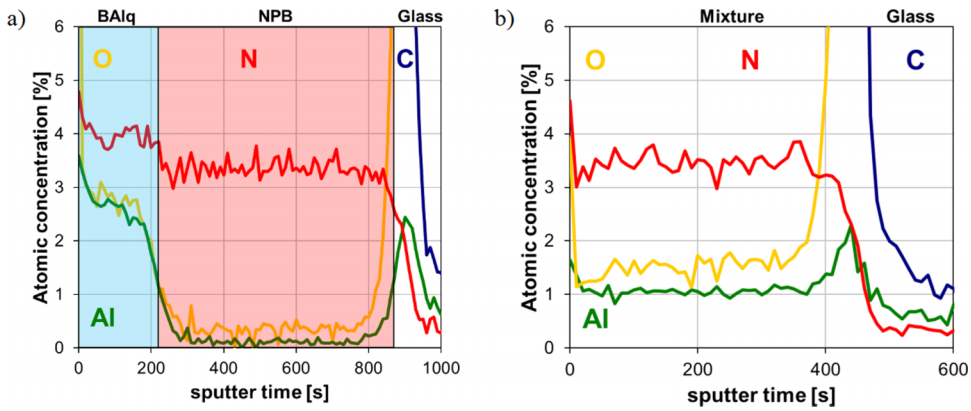

FIG. 8. XPS sputter depth profiles of slot die coated double layers of NPB and BAlq onto glass substrates: 8(a) Defined interface – BAlq is coated with EtOH as an orthogonal solvent for NPB, 8(b) Mixture – BAlq is coated with TOL as a non-orthogonal solvent for NPB.

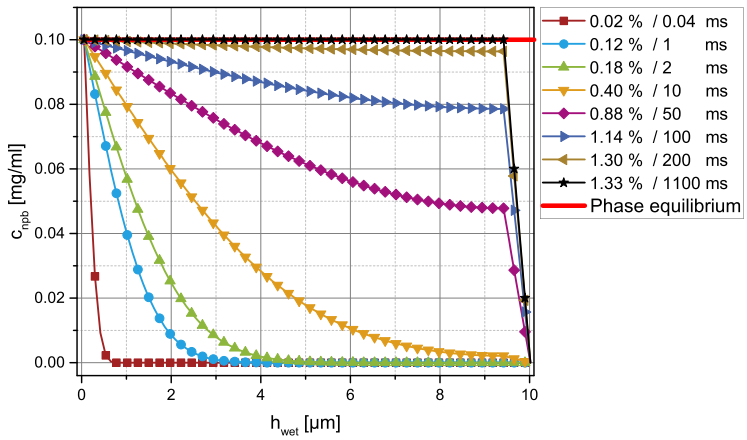

FIG. 9. Simulated concentration of dissolved NPB in a 10 µm EtOH film. The amount of dissolved solid NPB film of 60 nm is given in percentage and the respective time it takes until this stage of dissolution is reached.

earlier than for the reference device. This is in accordance with our experimental observations that the slot die coated films were several nanometers thinner than the knife coated ones.

Considering a NPB film thickness of 60 nm in the calculations as well as in the experiments, one expects the total NPB film to dissolve in TOL and only to an extent of 1.38 % in EtOH. This confirms that the experimental observations are in accordance with the thermodynamic boundaries set by the phase equilibrium. It is of interest that the limitations from the point of a high solubility can be overcome by changing drying conditions. The question is whether a setup can be found where drying kinetics dominate over the diffusion kinetics.

The calculated drying rate $\dot{m}_i$ (eq. (6) for a TOL layer of 3.2 g/(m^2·s) or 3.9 µm/s results in a calculated drying time (eq. (7)) for the second layer (h_{wet} = 10 µm) of 2.6 s, and for EtOH a rate of 6.6 g/(m^2·s) or 8.7 µm/s results in 1.1 s.

The diffusion coefficient needs to be known for calculating the diffusion kinetics. Therefore, the diffusion coefficient of NPB was measured by means of nuclear magnetic resonance for a high solvent content (D_{NPB} = 6.37E-10 m^2/s = 637 µm^2/s for $x_{Chloroform}$ = 99.3 %) and shows a value similar to liquids.[40] The concentration profiles of NPB are plotted in mg/ml over the film height for different time steps. The corresponding percentage of the dissolved dry film is given for every time step. The red line shows the phase equilibrium concentration of NPB in each solvent. The decrease of solid concentration at the top of the wet film is due to the boundary condition. Parameters applied in the simulation can be found in the supplementary information.[37]

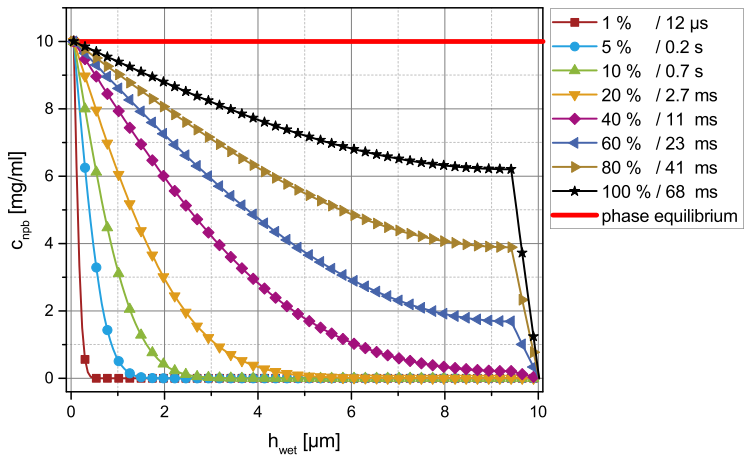

FIG. 10. Simulated concentration of NPB dissolved in a 10 µm TOL film. The amount of dissolved solid NPB film of 60 nm is given in percentage and the respective time it takes until this stage of dissolution is reached.

TABLE I. Comparison of XPS measurements and simulations.

Case	Thermodynamics	Drying time 2nd layer	Diffusion kinetics	Expectation from simulation	Experimental results
Orthogonal	0.8 nm of NPB dissolved	1.1 s	1.3 % of solid dissolved after 1.1 s	No intermixing	Defined double-layers
Non-orthogonal	NPB dissolved	2.6 s	Everything dissolved after 68 ms and factor 100 x faster than for orthogonal case	Completely intermixed	Completely intermixed

Figure 9 shows the dissolution of NPB in a wet film of EtOH, which is the case for the orthogonal solvent approach. The first molecules reach the solvent surface in 10 ms. The concentration of NPB increases quickly. After 100 ms, around 1 % of the NPB film is dissolved. Phase equilibrium is almost reached after 200 ms. As expected, an increase in diffusion time does not increase the NPB concentration further. In total, a very small amount of 1.33 % is dissolved in EtOH. This demonstrates that the NPB concentration in a BAlq film cast from EtOH cannot exceed ~ 1.3 % and, therefore, sharp interfaces are created.

The profile for the dissolution of NPB in the TOL wet film is shown in Figure 10. As expected, the NPB is dissolved completely. A diffusion of the solved material to the surface of the second layer takes place in ms. While it takes 100 ms in the case of EtOH to dissolve 1 % of solid, only 12 µs are required for TOL. It takes only 68 ms to dissolve the underlying NPB layer completely. Due to the high solubility and high concentrations gradients the Fickian diffusion is a factor 100 times faster than for the case of EtOH. Within the drying time of the TOL layer of 2.6 s, the fast diffusion results in equalization of the concentration profiles.

The experimental results and the calculations are summed up in Table I.

Experiments and calculations coincide completely for both cases. The orthogonal solvent case states that diffusion takes place slower than the non-orthogonal one. Nevertheless, it is still faster than the drying kinetics and a very small amount of NPB is distributed in the whole wet film. Due to the limited solubility, this does not account and no intermixing to a severe extent is expected. This is validated in the experiments. Applying the non-orthogonal solvent, the XPS measurement shows one fully intermixed layer. From the point of the phase equilibrium, this is expected. The higher drying time and the very fast diffusion kinetics predict that a complete intermixing has to occur.

Homogeneous layers can be coated by using non-orthogonal solvents, but this leads to an intermixing of the materials during the process and, subsequently, to a possible loss of the device function. The theoretical analysis states that the mixing of the OLED materials shown experimentally cannot be avoided for non-orthogonal solvents by adjusting the process conditions, e.g. by faster drying. This points out that even powerful industrial dryers with a heat transfer coefficient of 100 W/(m^2·K), which decreases the drying time by a factor of 10, will not prevent the intermixing. Solubility is the key parameter for the fabrication of solution-processed small molecule devices. Therefore, it can be concluded that the phase equilibrium and not diffusion and drying kinetics are of importance for the intermixing processes.

Diffusion takes place too rapidly due to the high diffusion coefficients, the high solvent contents of the coating liquids and the short diffusion lengths of the coated layers. Therefore, the non-orthogonal process regime is not suitable for the fabrication of OLEDs requiring separated layers.

IV. CONCLUSION AND OUTLOOK

Homogeneous small molecule OLED double layers were produced by the large-scale coating techniques of blade and slot die coating applying appropriate process parameters. A defined separated interface is created by using orthogonal solvents for two consecutive layers and has been proven by adequate characterization methods. A simplified model was introduced for calculating interdiffusion and drying kinetics, confirming the experimental observations. The calculations state

the importance of the solubility of the materials due to rapid diffusion. We conclude that it is not possible to create layers without or with only a small area of dissolution through non-orthogonal solvents for the coating and drying parameters investigated. Ongoing investigations focus on the simultaneous coating of the two materials with a two-layer slot die coater.

ACKNOWLEDGEMENTS

The authors acknowledge financial support via the project PrintOLED (contract number 13N10759 and 13N12280) of the Leading-Edge Cluster Forum Organic Electronics managed by InnovationLab GmbH within the High-Tech Strategy for Germany of the Federal Ministry of Education and Research and Philips Technologie GmbH. Special thanks goes to our cooperating partners BASF for evaporating reference samples. We would like to thank all mechanics, assistants and our students involved for contributing to this work. We acknowledge support from the Deutsche Forschungsgemeinschaft and Open Access Publishing Fund of Karlsruhe Institute of Technology.

NOMENCLATURE

Letters

c_i	Concentration of i	mg/ml
$\tilde{c}_{p,i}$	Molar heat capacity of i	J/(mol·K)
D	Diffusion coefficient of i in j	m^2 /s
h	Height (z-axis)	µm
Le	Lewis number	
$\dot{m}$	Mass flux or drying rate	g/(m^2·s)
M	Stability factor	-
$\tilde{M}$	Molar mass	g/mol
N	Factor for air flow	-
$\dot{n}$	Molar flux	mol/(m^2·s)
$\tilde{y}$	Molar fraction in gas phase	-

Greek Letters

α	Heat transfer coefficient	W/(m^2·K)
β_{ij}	Mass transfer coefficient of i in j	m^2 /s
Δ	Discrete difference	-
ρ	Density	g/cm^3
$\tilde{\rho}$	Molar density	mol/m^3
ϕ	Volume fraction	-

Indices

Dry	Drying
G	Gas phase
I	Component i
J	Component j
P	Isobar (p = constant)
Ph	Phase (at the interface)
solid	Solid
T	Actual time step
t+1	Next time step
wet	Wet
∞	In infinite distance
Z	At element z
z+1	At element z+1
z-1	At element z-1

[1] S. Höfle, H. Do, E. Mankel, M. Pfaff, Z. Zhang, D. Bahro, T. Mayer, W. Jaegermann, D. Gerthsen, C. Feldmann, U. Lemmer, and A. Colsmann, Organic Electronics **14**, 1820–1824 (2013).
[2] S. Tekoglu, G. Hernandez-Sosa, E. Kluge, U. Lemmer, and N. Mechau, Organic Electronics **14**, 3493–3499 (2013).
[3] S. R. Forrest, Chemical Reviews **97**, 1793–1896 (1997).
[4] S. Sax, N. Rugen-Penkalla, A. Neuhold, S. Schuh, E. Zojer, E. J. W. List, and K. Müllen, Advanced Materials **22**, 2087–2091 (2010).
[5] A. C. Grimsdale, K. L. Chan, R. E. Martin, P. G. Jokisz, and A. B. Holmes, Chemical Reviews **109**, 897–1091 (2009).
[6] J. Willmann, D. Stocker, and E. Dörsam, Organic Electronics **15**, 1631–1640 (2014).
[7] K. Kawano, K. Nagayoshi, T. Yamaki, and C. Adachi, Organic Electronics **15**, 1695–1701 (2014).
[8] H.-W. Chang, Y.-T. Lee, M.-R. Tseng, M.-H. Jang, H.-C. Yeh, H.-F. Meng, C.-T. Chen, Y. Chi, Y. Qiu, L. Duan, H.-W. Lin, S.-F. Horng, and H.-W. Zan, Synthetic Metals **196**, 99–109 (2014).
[9] C.-H. Jun, S. Ohisa, Y.-J. Pu, T. Chiba, and J. Kido, Journal of Photopolymers Science and Technology **28**, 343–347 (2015).
[10] A. Perumal, H. Faber, N. Yaacobi-Gross, P. Pattanasattayavong, C. Burgess, S. Jha, M. A. McLachlan, P. N. Stavrinou, T. D. Anthopoulos, and D. D. C. Bradley, Advanced Materials **27**, 93–100 (2014).
[11] A. R. G. Smith, K. H. Lee, A. Nelson, M. James, P. L. Burn, and I. R. Gentle, Advanced Materials **24**, 822–826 (2012).
[12] M. Eritt, C. May, K. Leo, M. Toerker, and C. Radehaus, Thin Solid Films **518**, 3042–3045 (2010).
[13] L. Duan, L. Hou, T.-W. Lee, J. Qiao, D. Zhang, G. Dong, L. Wang, and Y. Qiu, Journal of Materials Chemistry **20**, 6392 (2010).
[14] A. Elschner, H. W. Heuer, F. Jonas, S. Kirchmeyer, R. Wehrmann, and K. Wussow, Advanced Materials Research News **13**, 1811–1815 (2001).
[15] S.-R. Tseng, H.-F. Meng, C.-H. Yeh, H.-C. Lai, S.-F. Horng, H.-H. Liao, C.-S. Hsu, and L.-C. Lin, Synthetic Metals **158**, 130–134 (2008).
[16] T. Earmme and S. A. Jenekhe, Journal of Materials Chemistry **22**, 4660 (2012).
[17] T. Chiba, Y.-J. Pu, and J. Kido, Advanced Materials **27**, 4681–4687 (2015).
[18] H. Gorter, M. Coenen, M. Slaats, M. Ren, W. Lu, C. J. Kuijpers, and W. A. Groen, Thin Solid Films **532**, 11–15 (2013).
[19] K. H. Kim, J. Y. Lee, T. J. Park, W. S. Jeon, G. P. Kennedy, and J. H. Kwon, Synthetic Metals **160**, 631–635 (2010).
[20] J. Park, T. Park, W. Jeon, R. Pode, J. Jang, J. Kwon, E. Yu, and M. Chae, Organic Electronics **10**, 189–193 (2009).
[21] J.-D. You, S.-R. Tseng, H.-F. Meng, F.-W. Yen, I.-F. Lin, and S.-F. Horng, Organic Electronics **10**, 1610–1614 (2009).
[22] C.-Y. Chen, H.-W. Chang, Y.-F. Chang, B.-J. Chang, Y.-S. Lin, P.-S. Jian, H.-C. Yeh, H.-T. Chien, E.-C. Chen, Y.-C. Chao, H.-F. Meng, H.-W. Zan, H.-W. Lin, S.-F. Horng, Y.-J. Cheng, F.-W. Yen, I.-F. Lin, H.-Y. Yang, K.-J. Huang, and M.-R. Tseng, Journal of Applied Physics **110**, 94501 (2011).
[23] H.-C. Yeh, H.-F. Meng, H.-W. Lin, T.-C. Chao, M.-R. Tseng, and H.-W. Zan, Organic Electronics **13**, 914–918 (2012).
[24] M. Y. Lim, W. Yunus, Z. A. Talib, A. Kassim, C. F. Dee, and A. Ismail, American Journal of Engineering and Applied Sciences **3**, 64–67 (2010).
[25] F. Lindla, M. Boesing, P. van Gemmern, D. Bertram, D. Keiper, M. Heuken, H. Kalisch, and R. H. Jansen, Applied Physics Letters **98**, 173304 (2011).
[26] M. Carvelli, A. van Reenen, R. Janssen, H. P. Loebl, and R. Coehoorn, Organic Electronics **13**, 2605–2614 (2012).
[27] G. Mao, Z. Wu, Q. He, B. Jiao, G. Xu, X. Hou, Z. Chen, and Q. Gong, Applied Surface Science **257**, 7394–7398 (2011).
[28] N. R. Park, G. Y. Ryu, D. H. Lim, S. J. Lee, Y. K. Kim, and D. M. Shin, Journal of Nanoscience and Nanotechnology **14**, 5109–5113 (2014).
[29] S. Scholz, Q. Huang, M. Thomschke, S. Olthof, P. Sebastian, K. Walzer, K. Leo, S. Oswald, C. Corten, and D. Kuckling, Journal of Applied Physics **104**, 104502 (2008).
[30] B.-Y. Yu, Y.-Y. Chen, W.-B. Wang, M.-F. Hsu, S.-P. Tsai, W.-C. Lin, Y.-C. Lin, J.-H. Jou, C.-W. Chu, and J.-J. Shyue, Analytical Chemistry **80**, 3412–3415 (2008).
[31] K. Peters, L. Wengeler, P. Scharfer, and W. Schabel, Journal of Coatings Technology and Research **11**, 75–81 (2014).
[32] M. Baunach, S. Jaiser, S. Schmelzle, H. Nirschl, P. Scharfer, and W. Schabel, Drying Technology **34**, 462–473 (2015).
[33] K. L. Parry, A. G. Shard, R. D. Short, R. G. White, J. D. Whittle, and A. Wright, Surface and Interface Analysis **38**, 1497–1504 (2006).
[34] J. H. Scofield, Journal of Electron Spectroscopy and Related Phenomena **8**, 129–137 (1976).
[35] S. Tanuma, C. J. Powell, and D. R. Penn, Surface and Interface Analysis **21**, 165–176 (1993).
[36] P. J. Cumpson, J. F. Portoles, N. Sano, and A. J. Barlow, Journal of Vacuum Science and Technology B **31**, 21208 (2013).
[37] See supplementary material at http://dx.doi.org/10.1063/1.4953845 for the calculations of the solubility, Supplemental material A and for the modeling of diffusion and drying, Supplemental material B.
[38] *VDI-Wärmeatlas*, 10th ed., edited by Verein Deutscher Ingenieure (Springer-Verlag, Berlin, Heidelberg, New York, 2006).
[39] E.-U. Schlünder, *Einführung in die Stoffübertragung: Lehrbuchreihe Chemieingenieurwesen-Verfahrenstechnik* (Vieweg, Braunschweig, Wiesbaden, 1996).
[40] W. Schabel, *Trocknung von Polymerfilmen: Messung von Konzentrationsprofilen mit der Inversen-Mikro-Raman-Spektroskopie* (Universität Karlsruhe (TH), Shaker, Aachen, 2004).